Influence of reinforcing particle distribution on the casting characteristics of Al-SiC_p composites

Xinliang Yang[a,]*, Nilam S. Barekar[a], Shouxun Ji[a], Brij K. Dhindaw[b], Zhongyun Fan[a]

[a] BCAST, Brunel University London, Uxbridge, UB8 3PH, UK [b] School of Minerals Metallurgical and Materials Engineering, Indian Institute of Technology Bhubaneswar, 751013, India

ABSTRACT

Keywords:
Metal matrix composites (MMCs) Intensive melt shearing Particle distribution Fluidity Mechanical properties

SiC particulate reinforced A356 alloy metal matrix composites (MMCs) are synthesized using intensive melt shearing. The effect of reinforcing particle distribution on the fluidity of cast A356/10 vol.% SiCp composites is studied. Spiral length representing the fluidity of the composite melt was measured and liquid flow and solidification behaviour were analysed. Improvement in the fluidity of composites is attributed to the uniform distribution of reinforcing particles by intensive melt shearing treatment. From the casting performance point of view, uniform dispersion of reinforcing particles achieved with the aid of intensive shearing improves the mechanical properties of A356/10 vol.% SiCp cast composites. Improved strength, rigidity and wear resistance of composites is attributed to the bulk homogeneity, significantly reducing casting defects.

1. Introduction

Particulate reinforced Metal Matrix Composites (PRMMCs) have excellent isotropic properties compared to other MMCs due to the 3dimensionally distributed reinforcing particles in the matrix. With the combination of light metal matrix and stiff ceramic/metallic particles, a large variety of specific properties can be tailored exhibiting improved performance. To list a few, high elastic modulus above 120 GPa in 7091/SiCp MMCs (Jeong et al., 1990), high wear resistance (Nieto et al., 2017), and improved thermal conductivity of 135.1 ± 5.8 $Wm^{-1}K^{-1}$ (Miranda et al., 2018) with 1.5 vol.% addition of Cu-coated carbon fibres. Zhang et al. (1994) synthesized 6061/SiCp MMC presenting higher damping capacity compared to the matrix alloy, and Matsumoto et al. (2003) utilized ZrW2O8 particles to further reduce the thermal expansion coefficient of aluminium due to its negative thermal expansion properties.

The powder metallurgy (P/M) method is the mainstream commercial process for PRMMCs fabrication (Harrigan, 1998). The products are generally provided in billet form which go through complicated and energy intensive thermo-mechanical processes, which are then further machined into the desired shapes. Amongst the liquid melt fabrication methods summarized by Lloyd (1994), PRMMCs by melt processing (casting) is a promising manufacturing route that meets the complex geometrical requirement of components for aerospace, aviation, and ground transportation industries (Kainer, 2006). Taylor (1996) suggested that the structural integrity and metallurgical consistency of composite casting are mainly determined by the reinforcing particle dispersion and the feeding of the composite melt into the mould cavity that is controlled by its fluidity.

Due to the importance of the fluidity of the composite melt in the casting process, Ravi et al. (2008) reviewed the effect of size, volume fraction, distribution, and agglomeration of reinforcing particles on the fluidity of composite melts. In addition to this, Hashim et al. (2001) studied the relationship of the wetting of particles in the liquid matrix and the nature of composite fluidity. It has been well established that, for a given particle size, the specific fluidity decreases with an increase in volume fraction of reinforcement particles suspended in the melt, for example Al/Al2O3 (Emamy et al., 2009), and Al/SiC (Behera et al., 2012). Yarandi et al. (1993) studied the effect of reinforcing particle size on the fluidity and showed that the fluidity was decreased with the addition of smaller particles. The reason can be that the larger total surface area generated by smaller particles under same volume fraction can more effectively resist to flow due to the stagnant boundary layers around the particles. Timelli and Bonollo (2007) pointed out that increasing casting temperature is effective in improving the fluidity of the PRMMC

melt. However, Sritharan et al. (2001) observed that the formation of Al4C3 is enhanced by increasing the casting temperature of an Al-SiCp composite, which results in an increase in volume fraction and hence surface area of the suspended particles. It is consistent with Lloyd's work (1989) on the study of the particle interface with liquid matrix, which suggests that the chemical reaction between the reinforcement and the matrix alloy affects the fluidity of composite melt. Over the years, fluidity has been studied extensively from various angles and perspectives. However, despite the studies done so far, there is still limited understanding of the PRMMC melt fluidity in terms of the agglomeration of the reinforcing particles on the composite fluidity. This might be related to the technological limitation of tailoring particle distribution and dispersion in the melt of MMCs. Therefore, it is important to understand the role of particle clustering/agglomeration on the fluidity of the PRMMC melt.

Fan et al. (2016) developed a liquid metal treatment known as intensive melt shearing achieved through the rotor-stator mechanism and it is characterised by the uniformity of temperature and potential nuclei distribution. According to previous studies of high shear in an MMC melt (Fan et al., 2011), the applied shearing force should overcome the cohesive force holding particles in clusters/agglomerates, dispersing them into discrete individuals due to the intense turbulent flow generated within the melt. Moreover, Patel et al. (2013) showed that intensive melt shearing is capable of eliminating the vortex formation that normally appears with impeller-based mechanical stirring and thus maintains a stable melt surface while creating high turbulence inside the melt.

In the work presented in this study, intensive melt shearing generated by the rotor-stator mechanism and conventional impeller stirring were applied to fabricate an A356/10 vol.% SiCp composite reinforced by three different particle sizes. The particle distribution within the composites, was investigated in order to understand its effect on the casting characteristics, such as fluidity of the composite melt and the mechanical properties of the cast composites.

2. Experimental procedure

Norton Aluminium Ltd, Staffordshire, provided a commercial A356 alloy with a chemical composition of 6.76 wt% Si, 0.45 wt% Mg, 0.11 wt% Ti and balance Al. The silicon carbide particles (SiCp) used in the present work as reinforcement was provided by Electro Abrasives Corporation, NY, USA. These angular shaped black ⟨-SiC particles have a hexagonal crystal structure (ICSD 156190) with F500, F600 and F1000 particle sizes (equivalent to mass media particle size of 12.8 μm,
9.3 μm and 4.5 μm, respectively). The X-ray diffraction spectrums (Bruker D8 Advance) and detailed morphology of these SiC particles are presented in Fig. 1.

The matrix alloy was melted at 750 °C (TliquidusA356 ~ 615 °C), under a Nitrogen protective atmosphere, in a clay-graphite crucible, which was heated in an induction furnace. A total of 2.5 kg of the A356 alloy was prepared for melting and a small block of the alloy was added for melt temperature adjustment. The melting of the A356 alloy by induction furnace was achieved within 10 min. to minimize the hydrogen absorption. A pre-heated block of A356 alloy was put into the molten alloy to reduce the temperature of the A356 alloy melt to 600 °C thereby facilitating the reinforcing particles addition in the semi-solid state (A356 alloy solidus ~ 555 °C). SiCp particles were preheated at 400 °C for 1 h before adding to remove the moisture. The fabrication route of A356/10 vol.% SiCp composites is presented schematically in Fig. 2.

The fabrication of A356/10 vol.% SiCp composites was conducted in two stages. Firstly, the SiC particles were introduced into the A356 alloy melt held at 600 °C with the help of mechanical stirring, using a 45° four-bladed impeller, rotating at 650 rpm for 5 min.. The stainless steel impeller was coated with Boron Nitride and preheated at 200 °C before inserting it in the melt. Then the initially prepared A356/10 vol. % SiCp composite was heated to 730 °C and was subjected to the intensive melt shearing using a 40 mm diameter rotor-stator mixer for 5 min.. During the melt treatment, a speed of 5000 rpm was used to disperse the reinforcing particles in the melt. The composite melt was then poured into a spiral mould (Lin et al., 2001)(Fig. 3) at 730 °C to measure fluidity, in addition to a preheated steel mould complying with the guidance of ASTM E8/E8M-2013 standard, for tensile sample preparation. For comparison, mechanical stirring generated by impeller was also utilised in the same manner but with a 650 rpm rotation speed. For abbreviation, composite samples prepared with intensive melt shearing are referred to as HS and the reference samples prepared by impeller stirring are referred to as nonHS.
A356/10 vol.% SiCp composites for microstructural observations were sectioned from the grip area of the tensile bars. The fluidity test samples were taken from a section of the middle of the spiral tip along the flow direction. Metallographic samples were prepared following the standard route with a final polishing by OP-S suspension (0.05

μm water-based SiO_2 suspension). For electro-polishing, an electrolyte of 30 % HNO_3 in Methanol solution was used to prepare the spiral tip samples at −30 °C with a voltage of 12 V for 20 s.
A Carl Zeiss, AxioScope A1, optical microscope was used for particle distribution evaluation. A Zeiss Supra 35 field-emission gun SEM equipped with energy-dispersive X-ray spectroscopy (EDS) and electron backscattered diffraction (EBSD) camera (EDAX Ltd.) was used for detailed microstructural observations. For the quantification of the reinforcing particle distribution, the Quadrat method (Rogers, 1974) was employed on 5 optical micrographs of each sample with a given 8 × 8 quadrat grid covering a sample field of 416 μm × 416 μm.
Mechanical properties were measured on an Instron 5500 Universal Electromechanical Testing System with a constant crosshead speed of 1 mm/min and Bluehill® software for test control. The gauge dimensions of tensile samples of Φ 12.5 mm × 50 mm were determined according to the ASTM E8/E8M-2013 standard. For each condition, 4 tensile samples were tested. All the tests were performed at ambient temperature (∼25 °C). Brinell hardness test was performed on a Wilson BH3000 (Buehler, UK) Brinell hardness tester with a load of 250 kgf, load time of 5.0 s and dwell time of 15 s. Samples for Brinell hardness test were machined from the cylindrical bars located next to the tensile samples and then ground with 75 μm diamond coated grinding disc for a smooth surface. Dry sliding abrasion wear tests were carried out on a pin-on-disk wear test apparatus. 8 mm diameter cylindrical samples were held against a rotating disk having a 500 grit SiC paper with 1 kg load. A wear track with a 128 mm diameter is used to provide 1 m/s sliding velocity. Wear loss was calculated from the weight loss of the cylindrical sample at 250 m sliding distance intervals.

3. Results and discussion

3.1. Particle distribution

The microstructure of the as-cast A356/10 vol.% SiCp composites with different particle sizes and melt treatments are presented in Fig. 4. An improved uniform spatial distribution of reinforcing particles in HS samples was visible compared with that in the non-HS samples. For the intensively sheared samples, as shown in Fig. 4(a) and (c), the SiC particles were located in the inter-dendritic regions and grain boundary areas which form a fine network, with the agglomeration of particles rarely observed. With decreasing particle size to 4.5 μm(Fig. 4(e)), improvement of the distribution of SiC particles was observed in the HS sample compared to its counterpart. On the other hand, an increase of agglomerates with decreasing particle size was seen in the mechanically stirred samples (Fig. 4(b), (d) and (f)). For the impeller stirred composite sample with 4.5 μm sized particles (Fig. 4(f)), the reinforcement particles are mainly in the form of agglomerates with a wide range of cluster sizes. Although local dispersions of SiCp were revealed in both samples in a high magnification image, the intensively sheared sample shows more uniform particle dispersion.
Statistical analysis of particle distribution, uniformity and agglomerate size distribution, are depicted in Fig. 5, which is based on the particle spatial distribution and excluded the phase differences, located within the grain or grain boundary area. A lower value of Skewness

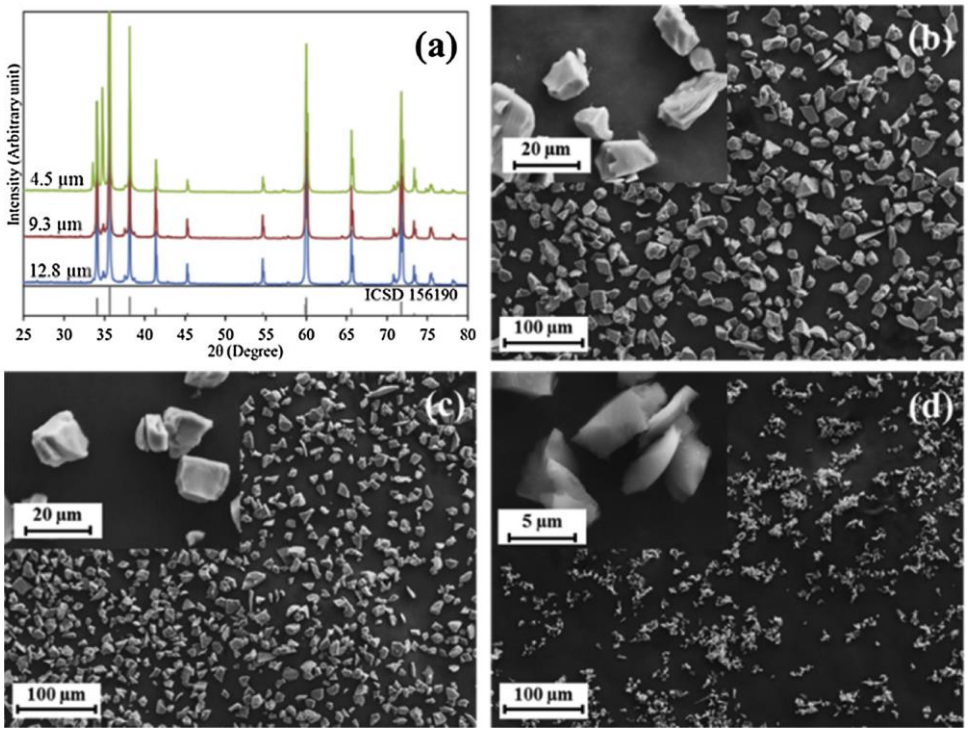

Fig. 1. The XRD analysis and morphology of ⟨-SiC particles with different particle size used for A356/10 SiCp composites fabrication.

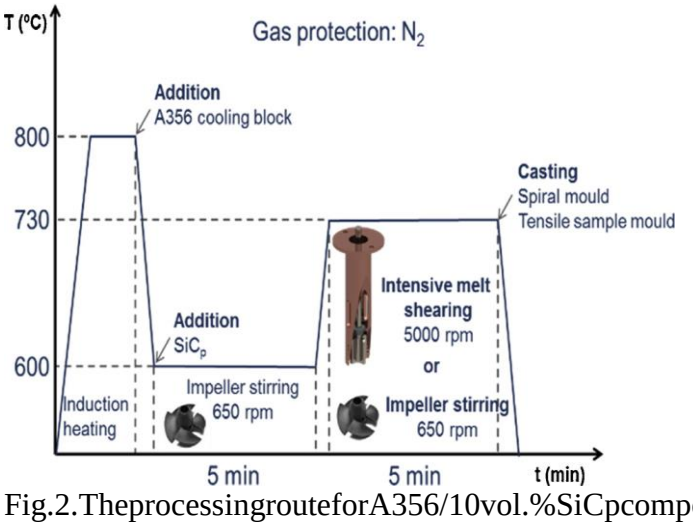

Fig.2.TheprocessingrouteforA356/10vol.%SiCpcompositeswithdifferentSiCparticlesizes.Twotypesofdispersingmethods,intensivemeltshearing(HS)andimpellerstirring(nonHS)wereusedforobtainingdifferentre-inforcementparticledistributions.

(Karnezis et al., 1998) represented a more uniform distribution of particles and a narrow range of agglomerate size (10~30 μm) is shown in HS samples with all three particle sizes. The above findings suggested that the high shear rate produced by the rotor-stator device could effectively break-up the agglomerates, which were initially formed while introducing the particles by impeller stirring in the semi-solid state. The break-up of the particle agglomerate/cluster is crucial for improving the dispersion of reinforcement particles in the composite melt.

In the case of melt treatment by the rotor-stator mechanism, the composite melt undergoes two-stage intensive shearing. The rotor rotates at a certain speed (10^3~10^4 rpm) within the stator and high shear stress is generated in the gap between rotor and stator. The shear stress (τ) can be estimated by the equation (Atiemo-Obeng and Calabrese, 2004):

$$\pi N D \tau = \eta$$

δ (1)

where η is the dynamic viscosity of the composite melt, N is the rotating speed of the rotor head, D is the diameter of rotor head and δ is the gap between the rotor head and the inside surface of the stator. By using the modified Einstein's equation developed by Guth and Simha (1936), the dynamic viscosity of A356/10 vol.% SiCp is calculated as 1.39×10^{-3} Pa·s. The shearing speed for the experiment was 5000 rpm. Thus, by using Eq. (1), the shear stress on the composite melt is calculated to be 443 Pa.

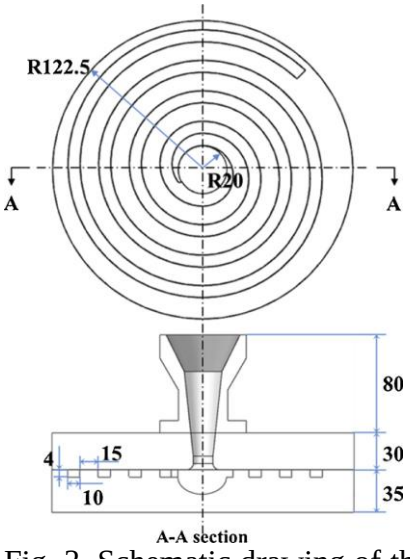

Fig. 3. Schematic drawing of the permanent spiral mould used for fluidity tests of A356/10 vol.% SiCp composites with different SiC particle sizes and composite melt treatments.

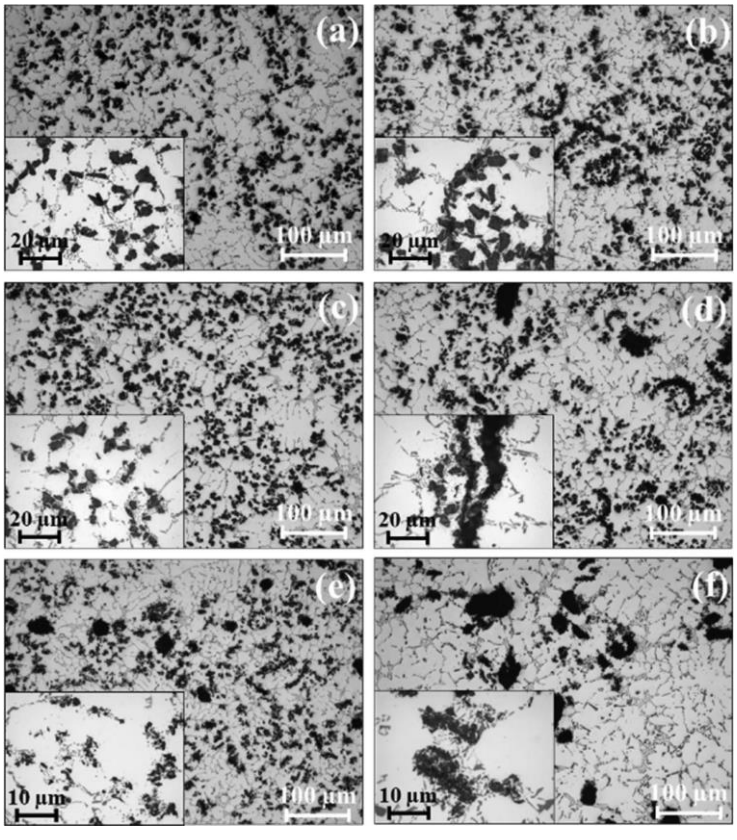

Fig. 4. The microstructure of as-cast A356/10 vol.% SiCp composites with detailed features of different particle sizes and composite melt treatments.

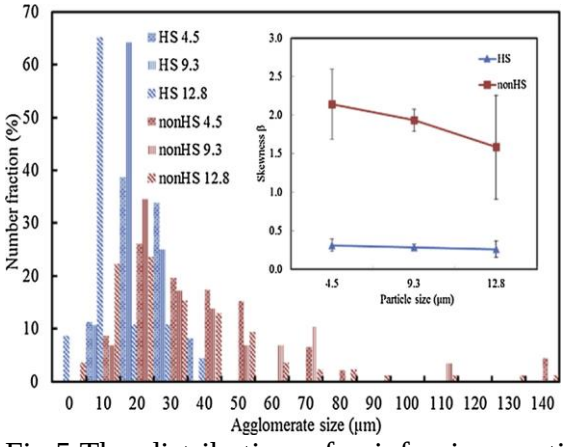

Fig.5.The distribution of reinforcing particles (Skewness β) determined by quadratmethodinA356/10vol.%SiCp composites fabricated with different SiC particle sizes and composite melt treatments.

After the composite melt is delivered into the gap between the rotor and stator, the liquid will be further ejected out through the apertures on the stator head at high speed. The shear stress (τ) on the composite melt through the stator aperture can be presented by the following Eq.
(2) (Douglas et al., 2011):

$$\tau = f\rho v^2/2 \quad (2)$$

where f is the flow friction factor which is 0.02 for turbulent flow in a pipe with smooth surface (the Moody chart (Douglas et al., 2011)), ρ is the fluid density and ϑ is the mean flow velocity. The theoretical density of A356/10 vol.% SiCp melt is 2.75 g/cm^3 which is calculated by the rule of a mixtures. Utomo et al. (2009) studied the approximate flow velocity of water in a similar rotor-stator mixer geometry and 10 m/s was adopted for the mean flow velocity. The shear stress experienced in a composite melt through a single stator aperture can be estimated as 2.75×10^3 Pa. Under these conditions, the shear stress is generated by a large velocity gradient through boundary layer effect between the inner wall surfaces of the aperture and the centre of the aperture hole. This shear phenomenon further breaks-up the SiC agglomerate/cluster.
Based on the calculations by (Rumpf's model, 1962), Yang et al. (2016) reported the tensile strength of agglomerates can be in the range of less than 10^2 Pa. The shear stress provided by the rotor-stator device is higher than the strength for holding SiC agglomerates and is capable of breaking them up. As the cluster tensile strength is inversely pro-

portional to the square of particle size ($T \propto \frac{F}{a^2}$), the smaller the particle size, the higher the strength of the cluster. With the same shear speed in the experiments, the 4.5 μm sized reinforcing particles are shown to exhibit a higher content of agglomerates compared to the composite

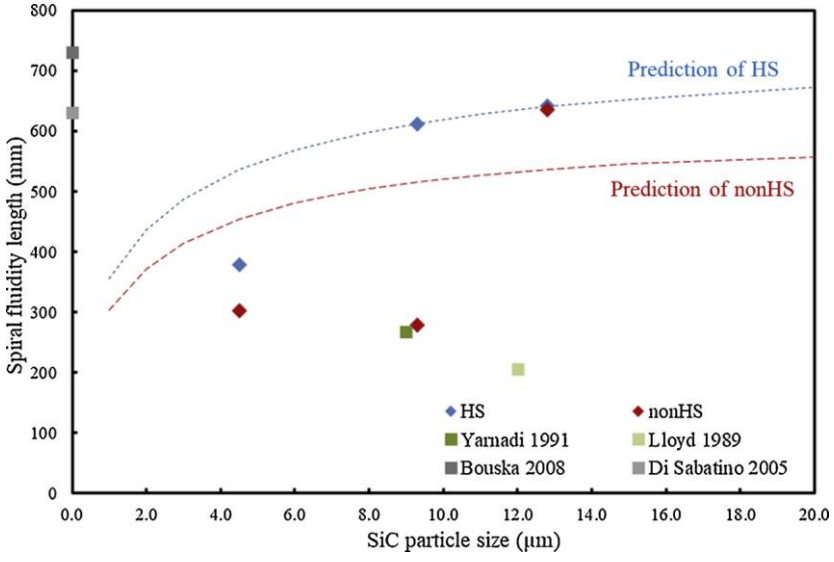

Fig. 6. The spiral fluidity length of as-cast A356/10volSiCp composites fabricated with different SiC particle sizes and composite melt treatments.

samples with larger sized reinforcement. So as the particle size of the reinforcement decreases, higher rotation speed is desirable in order to ensure a good dispersion of the reinforcements.

3.2. Fluidity

3.2.1. Results of spiral mould fluidity test

The spiral length of as-cast A356/10 vol.% SiCp composites with different SiC particle sizes is shown in Fig. 6. Campbell and Hardning (1994) pointed out that in general a longer spiral length indicates improved fluidity of the melt. A longer spiral length was observed in the cast sample treated by intensive shearing compared to the length of the sample by impeller stirring, thus suggesting an improvement in fluidity in the composite melt treated by intensive shearing. The spiral lengths of the composite melt incorporating 12.8 μm sized SiC particles with melt shearing treatment is significantly higher than the value of a similar composite reported by Lloyd (1989) and comparable to the value of monolithic alloys in similar conditions, AlSi7Mg0.3 alloy (Bouska, 2008) and Al-7Si alloy (Di Sabatino et al., 2005) cast at 730 °C. With the
9.4 μm sized SiC particles, the composite melt created a spiral length of 611 mm, which was close to the composite sample with 12.8 μm sized SiC particles (641 mm) treated with intensive shearing. However, the spiral length of the composite melt with 9.4 μm sized SiC particles treated only by impeller stirring reduced dramatically to 278 mm, which is consistent with Yarnadi's work, 1991). By adding 4.5 μm sized SiC particles, the spiral lengths of the composite melt reduced to 378 mm for the intensively sheared melt and 302 mm for the nonHS sample. The results of the spiral length test suggest that intensive melt shearing has improved the fluidity of the composite melts with different SiC particle sizes for the same volume fraction.

The microstructure and morphology of ⟨-Al at the tip of the spiral strip for both samples (9.3 μm particle size) with and without intensive melt shearing were revealed as depicted in Fig. 7. The grain size of the intensive shearing treated sample is 147.1 ± 33.1 μm, and the value of the sample without intensive shearing treatment is 169.7 ± 45.5 μm. A similar dendrite arm spacing of 29.4 ± 4.9 μm and 23.2 ± 3.8 μmis also observed for the HS and nonHS samples respectively. From the SEM secondary electron signal images (SE2) (Fig. 7(a) and (b)), a more uniform distribution of SiC particles is observed in the matrix at the tip of the spiral casting, prepared with intensive shearing when compared with the impeller stirred sample. The nonHS sample contains a high volume fraction of agglomerates and porosity, which is attributed to the insufficient dispersion and oxide films/gas dragged into the melt by the vortex during the mechanical stirring. Fig. 7(c) and (d)) represented the morphology of Al grain in the tip area of both HS and nonHS samples by the EBSD analysis. The ⟨-Al grain in HS sample shows an equiaxed dendritic morphology with a random crystallographic orientation. In contrast, irregular shaped ⟨-Al dendrites occur in the area where agglomerates exist and porosity is observed.

The influencing factors for the fluidity of MMCs are normally categorized as material variables, mould/casting

variables and test variables (Ravi et al., 2008). In the present study, the mould/casting variables and test variables are set to be constant; the difference in fluidity of the composite melt with and without intensive melt shearing would thus be areflection of the distribution of the reinforcement in the melt.

The relationship between the spiral fluidity length of the monolithic alloy to the metallurgical, thermal and fluid dynamical parameters developed by Flemings (1974) is presented below: where, *Cp i*s the specific heat of the liquid alloy, *d i*s the thickness of the casting, Δ*H*is the heat of fusion (latent heat) of the alloy, *h i*s the heat transfer coefficient between the mould, *Km* is the thermal conductivity of the mould, *Lf i*s the length of the spiral channel, *T i*s the temperature of metal, *T0*is the mould temperature, Δ*T*is the superheat, *V i*s the metal flow velocity, Δ*x*is the length of the zone at the tip of the flowing stream in which choking occurs, *αm* is the thermal diffusivity of mould and *ρi*s the density of liquid metal.

$$m\ critical_{), Ravi}$$

By incorporating the critical solid fraction of alloys。 The influence of interlock by the solid dendrites has been accounted for during the solidification. The length of fluid flow (*Lf*) would also depend on the pressure drop caused by the internal friction of fluid. By combining Poiseuille's equation (Douglas et al., 2011) with Eq. (5), the influence of viscosity of fluid flow on the spiral length can be expressed as pouring head due to high internal friction, leading to the reduced spiral Fig. 7. The SEM images and EBSD maps of spiral tips of as-cast A356/10 vol.% SiCp composites containing 9.3 μm sized SiC particles with and without intensive melt shearing. 22*ρdgHr k*2 *m* and nonHS samples of A356/10 vol.% SiCp composites shown a similar (6) where, *g* is the gravitational force, *η i*s the viscosity of the molten alloy, *H* is the height of the sprue, *r i*s the equivalent radius of channel cross-section and A is the experimental constant.

Compared with monolithic alloys, the fluidity of the composite melt would have to be calculated considering the influence of reinforcement during the casting in the spiral mould. effect of particle size on the spiral length as the larger particles lead to a longer spiral length. However, the agglomeration affects the viscosity of the composite flow significantly. According to Mooney (1951), a higher volume tends to be occupied by the particle agglomeration due to the trapped air and particle gap. Such a higher apparent volume fraction of reinforcement would be expected to reduce the viscosity of the composite. Furthermore, the increased viscosity weakens the casting's is the heat of fusion (or latent heat) of the composite and *Cc* is the specific heat of the composite. The detailed equation derivation is presented in the appendix.

By analysing Eq. (7), it can be deduced that the spiral length of the casting is influenced by two key stages from the moment the composites melt is poured into the inlet to the completion of solidification. The first stage is in the range when melt temperature above the liquidus of the matrix metal. During this stage, the composite melt flows through the spiral mould channel composing solid reinforcing particles and liquid metal. The second stage starts when the temperature of the composite melt drops below the liquidus of the matrix alloy. The solid fraction of the composite melt increases as the solidification of the matrix alloy progresses. Once the dendrite meets the neighbouring grains, the flow of the composite melt stops and the spiral mould casting terminates (Flemings, 1974).

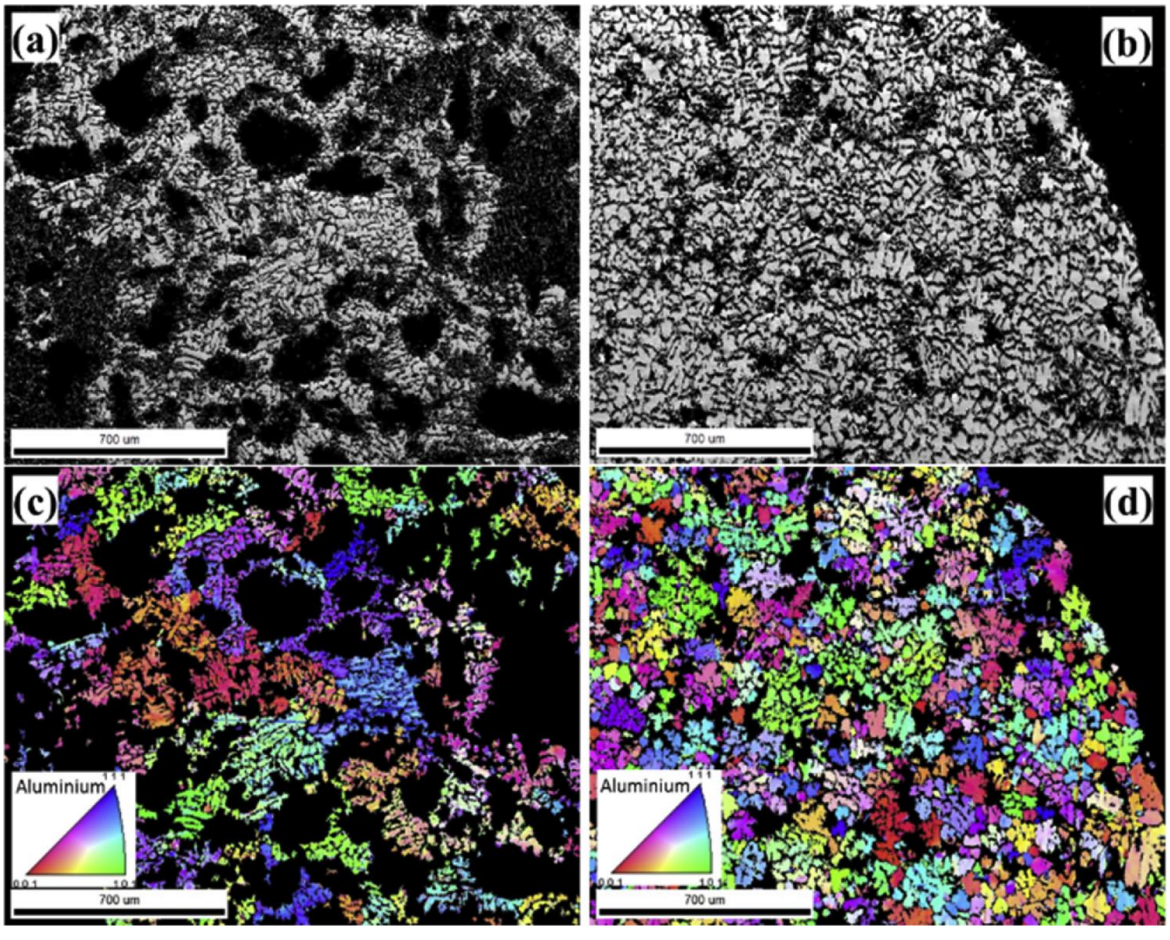

3.2.2. Stage 1: Tmelt≥T liquidus

From Eq. (7), when other parameters are set constant, an inverse proportional relationship between the viscosity of the composite flow and its spiral length is obtained. Wang et al. (2003) suggested that the viscosity of the composite rises with decreasing particle size when the length. The spiral length of intensive sheared composites are highly extended compared to impeller stirred samples because of the improved SiC particle dispersion.

3.2.3. Stage 2: Tmelt <Tliquidus

With the continuous heat extraction by the spiral mould during the composite melt flow, the temperature of the flow front is lower than the melt behind. The solidification of the primary Al phase is initiated at the tip of the composite melt flow, when the melt temperature reaches the matrix liquidus and attains its required undercooling. In the solidification of solute rich aluminium alloys, equiaxed dendrites grow into the undercooled melt until the liquid is completely consumed. However, after a certain period, primary dendrite tips impinge onto the neighbouring dendrites, which is identified as a dendrite coherency point (Dahle et al., 1996). The solid fraction of liquid alloy at this moment is defined as a critical solid fraction. Such a network of stiff dendrites contacting each other resists further macroscopic flow until it completely stops.

In the case of the impeller stirred composite melt, the agglomerates of SiC particles behave as a solid partition, occupying an excessive volume of the composite melt. So, an early coherency point is expected to stop the macro-flow, which is leading to the shorter spiral length. In Fig. 6, the theoretical calculation of the spiral length of composites is plotted to compare with experimental results. For a fixed volume fraction of reinforcing particle addition, a good fitting is observed with the experimental measurement of sheared composites. Since the rule of mixtures has been invoked for calculations of the physical properties and viscosity, assuming a uniform distribution of the particles, the particle distribution must be uniform for a good fit. The deviation of experimental results from the theoretical calculation for the 4.5 μm sized composite could be linked to the higher agglomerate content due to the increased cohesive force of finer sized particles (Lin et al., 2008). Therefore, with the same set of intensive

shearing parameters, the dispersing effect is more efficient in the composites with larger sized particles in the composite melt. The measured spiral lengths of the non-sheared sample are far below the theoretical calculation. Such a large deviation of experimental data from the impeller stirred sample is attributed to the non-uniform dispersion and presence of agglomerates in the composite melt. This is due to insufficient power input to counter cohesive forces holding SiCp clusters/agglomerates together.

By analysing the two stages of the spiral mould casting with composite melt, it is seen that the effect of the reinforcing particle dispersion by intensive melt shearing influences the total spiral length. This is due to the reduced viscosity of the composite melt and delayed coherency point of the ⟨-Al dendrites during the solidification of the matrix alloy. Such improvement of the spiral length reflects the increase in the composite fluidity, which assists the filling of composite melt into casting components with complicated geometries.

3.3. Mechanical properties

The major applications of particulate reinforced, aluminium alloy composite are utilising its advantages of high ultimate strength, elastic modulus and wear resistance compared to conventional materials (Kainer, 2006). It is important to reveal the impact of reinforcing particle dispersion on the mechanical properties of the cast composites.

3.3.1. Tensile properties

Fig. 8(a) shows the stress-strain curves of A356/10 vol.% SiCp composites of different SiC particle sizes, with and without intensive shearing treatment. Detailed mechanical properties of A356/10 vol.% SiCp composites are listed in Table 1.

An improved yield strength and ultimate strength have been observed in the intensively sheared sample with SiC particle size of 9.3 μm and 12.8 μm compared with the nonHS samples. As a similar grain size is observed in the HS and non-HS samples, the contribution of strengthening by grain boundary strengthening mechanism would be similar in both cases. Lloyd (1991) reported that the fracture of composite materials is associated with clusters or agglomerates which act as cracks or de-cohesion sites or both. Srivatsan et al. (2003) explained that the short inter-particle distance, facilitates the growth and linkage between neighbouring voids and microscopic cracks in the regions of particle clustering, or agglomeration. Sreekumar et al. (2015) reported that well-dispersed particles improve the integrity of the materials and a well-bonded SiC particle within the matrix raises the energy threshold for void formation and separation between the reinforcement and matrix. A schematic illustration of such influences is shown in Fig. 9. However, with a reduced SiC particle size to 4.5 μm, a similar tensile strength has been observed in both the samples with and without intensive shearing treatment. In such a condition, the sharply increased surface area and cohesive force (Rohatgi, 1980; Jones et al., 2003) hindered the intensive shearing in dispersing the particles, which leaves a higher defect content in both conditions compared to the samples with larger particle sizes.

By sharing a similar principle, the friction stir processing (FSP) method was reported to successfully fabricate a Cu matrix composite reinforced with nanoparticles (AK et al., 2015). The significantly increased shearing stress is arises from a dramatically increased matrix viscosity as the FSP was performed in the solid-state. Madhu et al. (2018) reported the fabrication of Al/TiO2 nanoparticle reinforced MMCs by ceramic particle fracturing in the FSP procedure, which suggests that the shearing stress generated in the process is even higher than the TiO2 particle strength. Enlightened by the FSP process, further improvement of shearing stress from the rotor-stator device by increasing the composite viscosity and/or rotation speed may enable the sub-micron and/or nanoparticle dispersion by intensive melt shearing treatment.

The relationship of the elastic modulus and the yield strength of composites prepared under different conditions is shown in Fig. 8(b). The intensively sheared samples present higher elastic modulus and yield strength with varying reinforcement particle sizes. An improvement in elastic modulus with intensive melt shearing compared to the impeller stirred samples with different SiC particle sizes, is clearly seen. This indicates that the uniform dispersion of SiC particles and defect control by breaking-up agglomerates lead to a higher strength and stiffness. The theoretical value of the elastic modulus of the composite can be calculated by the Rule of Mixtures. By using an elastic modulus of 72.4 GPa (ASM International, 1990) and 450 GPa (Wolfenden et al.,

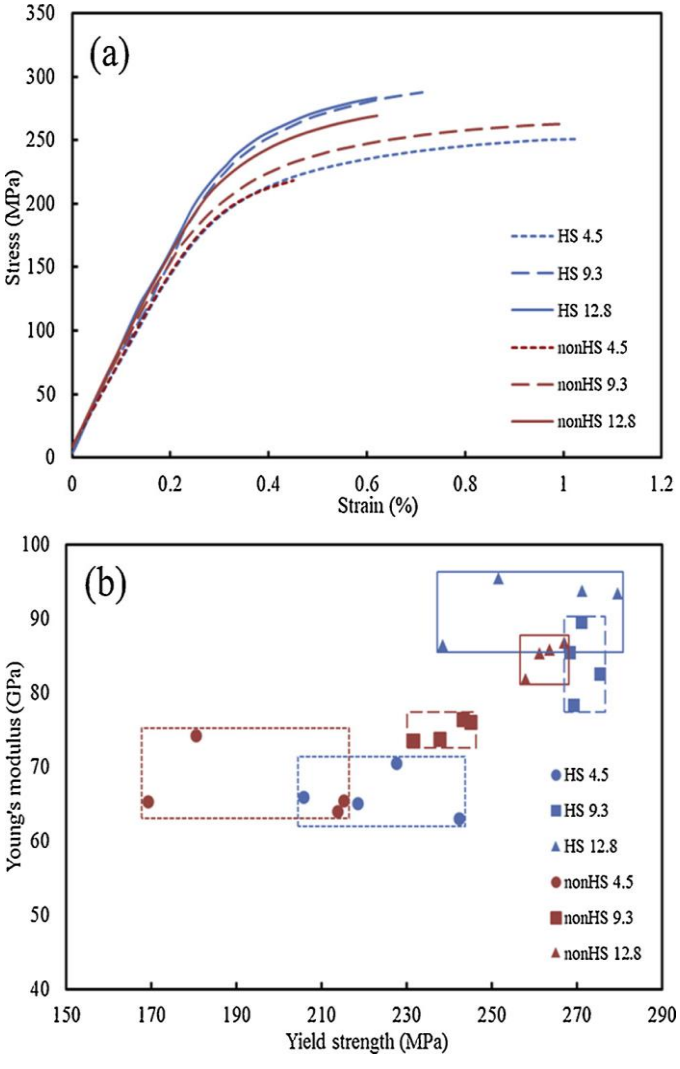

Fig.8.TensilepropertiesofA356/10vol.%SiCpcompositesfabricatedwithdifferentSiCparticlesizesandcompositemelttreatments.

Table1
TensilepropertiesofA356/10vol.%SiCpcompositesfabricatedwithdifferentSiCparticlesizeandcompositemelttreatments.

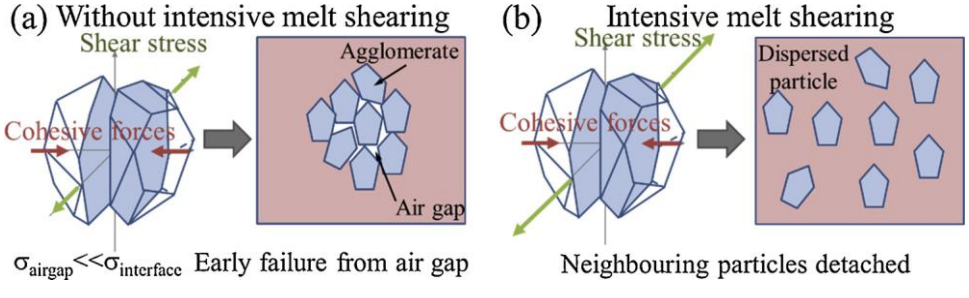

Fig. 9. The schematic illustration of the influence of intensive melt shearing on particle dispersion. 1996) for the A356 alloy and SiC, respectively, it is calculated that the elastic modulus of an A356/10 SiCp composite could reach 110.2 GPa in theory. The intensively sheared composite samples containing 12.8 μm SiC particles have an elastic modulus of 92.3 ± 4.1 GPa, which is closing to the theoretical value.

3.3.2. Hardness and wear resistance

Brinell macro-hardness measurements were carried out on the as-cast A356 alloy, and A356/10 vol.% SiCp composites containing 9.3 μm sized SiC particles prepared with and without intensive melt shearing (Fig. 10).

With the addition of SiC reinforcing particles, the Brinell hardness was improved significantly from 56.3 ± 1.7 HBW5/250 to above 65 HBW5/250 for the nonHS sample compared to monolithic alloy. Furthermore, with a well-dispersed reinforcement in the matrix in the intensively sheared composite samples, a hardness value of 71.9 ± 1.0 HBW5/250 has been achieved. Tjong and Lau (2000) recognised that an improved macro-hardness value indicates a higher wear resistance. Further dry sliding tests were performed and results are presented in Fig. 11. Wear resistance of A356/10 vol.% SiCp composite is under 0.06 vol.%/100 m for 4.5 μm particle addition comparing to nonHS sample of 0.16 vol.%/100 m. Indicated by Sannino and Rack (1995), composite samples with improved reinforcing particle distribution presented lower wear loss in the dry sliding test, while nonHS samples shown a higher wear loss with a reduction in reinforcement particle size. From the SEM images of the sliding surfaces, large agglomerates of SiC particles clustering together can be clearly seen, for the nonHS sample. With intensively sheared samples, SiC particles were uniformly dispersed on the worn surface thereby preventing sliding. Wear resistance of the composite is a strong function of volume fraction, size (Alpas and Zhang, 1992) and distribution (Thakur and Dhindaw, 2001; Barekar et al., 2009) of the reinforcing particles. Yalcin and Akbulut (2006) highlighted that the agglomeration of particulates deteriorates the abrasive resistance of the composite, as particles associated with clusters are only loosely bonded to the matrix and hence they are easily pulled out of the matrix during wear. Good bonding between the uniformly distributed SiCp and the matrix helps the reinforcement to be retained by the matrix, giving a reduced rate of abrasion.

Fig.10.TheBrinellhardnessofas-castmonolithicA356alloy,A356/10vol.%SiCpcompositefabricatedwithintensivemeltshearing(HS)andA356/10vol.%SiCpcompositefabricatedwithconventionalimpellerstirring(nonHS).

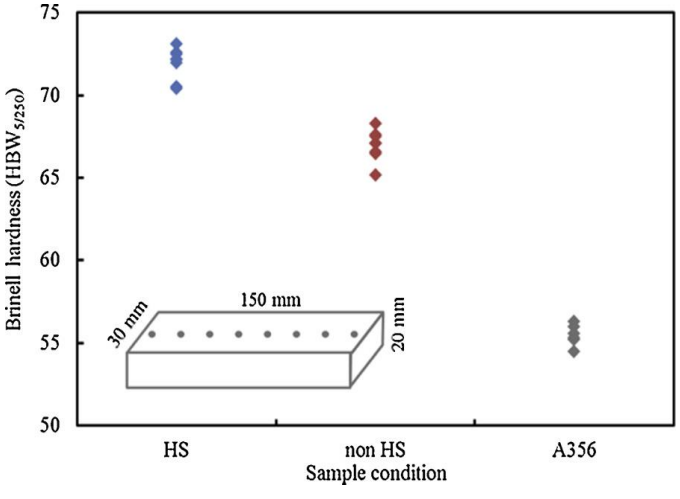

Fig.11.DryslidingweartestofA356/10vol.%SiCpcompositesfabricatedwithdifferentSiCparticlesizesandcompositemelttreatmentsandtheirsurfacemorphology.

In summary, the mechanical properties of A356/10 vol.% SiCp composites with an improved reinforcement particle distribution, as a result of intensive melt shearing, show superior strength, stiffness and wear resistance compared to the non-sheared samples.

4. Conclusions

An uniform distribution of SiC reinforcing particles through intensive melt shearing is achieved in the A356/10 vol.% SiCp composites processed with different particle sizes. The intense shearing force generated in the gap of rotor and stator as well as in the apertures on the stator wall, breaks up the SiC agglomerate/cluster into individually dispersed particles, uniformly distributing them in the ⟨-Al matrix.

The improved reinforcement particle distribution of A356/10 vol.% SiCp composite melt shows an increased spiral length during the mould filling, due to enhanced fluidity as a result of the reduction in the viscosity of the composite melt. The improved reinforcing particle distribution also increased the castability of the composite due to delayed coherency point of the ⟨-Al grain growth during solidification.

A356/10 vol.% SiCp composite with improved reinforcement particle distribution show increased strength, rigidity and wear resistance because of the improved structural integrity in the samples by uniform reinforcement dispersion

and improved defect control. With the
intensive shearing treatment, a high elastic modulus of 92.3 ± 4.1 GPa Acknowledgments is obtained in the composite with 12.8 μm particle addition and wear resistance of A356/10 vol.% SiCp composite is under 0.06 vol.%/100 m This work is supported by The Engineering and Physical Sciences for 4.5 μm particle addition comparing to nonHS sample of 0.16 vol. Research Council (EPSRC), UK, through the Towards Affordable, Close- %/100 m. Loop Recyclable Future Low Carbon Vehicle Structures (TARF-LCV)
programme, Grant No. EP/I038616/1. The authors would like to thank Declaration of Competing Interest Mr. Peter Lloyd in conducting intensive shearing experiments and Dr Brian McKay for constructive suggestions and proofreading in manu-
The authors declare that they have no known competing financial script revision from BCAST, Brunel University London. interests or personal relationships that could have appeared to influence the work reported in this paper.

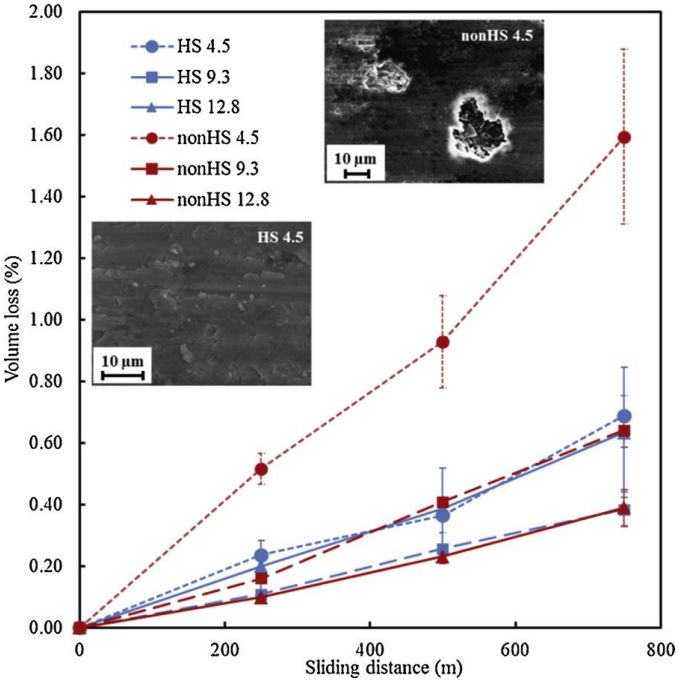

References

1) Alpas, A., Zhang, J., 1992. Effect of SiC particulate reinforcement on the dry sliding wear of aluminium-silicon alloys (A356). Wear 155, 83–104.
2) ASM International, ASM International, 1990. Handbook committee, ASM International. Alloy phase diagram committee. Metals Handbook: Properties and Selection. Asm International.
3) Atiemo-Obeng, V.A., Calabrese, R.V., 2004. Rotor–stator mixing devices. Handbook of Industrial Mixing: Science and Practice. pp. 479–505.
4) Barekar, N.S., Tzamtzis, S., Dhindaw, B.K., Patel, J., Hari Babu, N., Fan, Z., 2009. Processing of Aluminum-graphite particulate metal matrix composites by advanced shear technology. J. Mater. Eng. Perform. 18 (9), 1230–1240.
5) Behera, R., Chatterjee, D., Sutradhar, G., 2012. Effect of reinforcement particles on the fluidity and solidification behavior of the stir cast aluminum alloy metal matrix composites. Am. J. Mater. Sci. 2, 53–61.
6) Bouska, O., 2008. The effect of different casting parameters on the relationship between flowability, mould filling capacity and cooling conditions of al-si alloys. Metalurgija 14, 18–30.
7) Campbell, J., Hardning, R., 1994. The fluidity of molten metals. Training In Aluminum Application Technologies. TALAT Lecture 3205.
8) Dahle, A., Tøndel, P., Paradies, C., Arnberg, L., 1996. Effect of grain refinement on the fluidity of two commercial Al-Si foundry alloys. Metall. Mater. Trans. A 27, 2305–2313.
9) Di Sabatino, M., Syvertsen, F., Arnberg, L., Nordmark, A., 2005. An improved method for fluidity measurement by gravity casting of spirals in sand moulds. Int. J. Cast Met. Res. 18, 59–62.
10) Douglas, J.F., Gasiorek, J.M., Swaffield, J.A., Jack, L.B., 2011. Fluid Mechanics, sixth edition. Pearson Education Limited, Essex.
11) Emamy, M., Abbasi, R., Kaboli, S., Campbell, J., 2009. Fluidity of Al based metal matrix composites containing Al2O3 and SiC particles. Int. J. Cast Met. Res. 22, 430–437.
12) Fan, Z.Y., Zuo, Y.B., Jiang, B., 2011. A new technology for treating liquid metals with intensive melt shearing. Mater. Sci. Forum 690, 141–144.
13) Fan, Z., Jiang, B., Zuo, Y., 2016. Apparatus and Method for Liquid Metal Treatment. Apparatus and Method for Liquid Metals Treatment. US 13/823,216.
14) Flemings, M.C., 1974. Solidification Process. McGraw Hill, New York, USA.
15) Guth, E., Simha, R., 1936. Untersuchungen über die viskosität von suspensionen und lösungen. 3. Über die viskosität von kugelsuspensionen. Colloid Polym. Sci. 74, 266–275.
16) Harrigan, W.C., 1998. Commercial processing of metal matrix composites. Mater. Sci. Eng. A 244, 75–79.
17) Hashim, J., Looney, L., Hashmi, M.S.J., 2001. The wettability of SiC particles by molten aluminium alloy. J.

Mater. Process. Technol. 119, 324–328.
18) Jeong, H., Hsu, D.K., Shannon, R., Liaw, P., 1990. Elastic moduli of silicon carbide particulate reinforced aluminum metal matrix composites. Anonymous Review of Progress in Quantitative Nondestructive Evaluation. Springer, pp. 1395–1402.
19) Jones, R., Pollock, H.M., Geldart, D., Verlinden, A., 2003. Inter-particle forces in cohesive powders studied by AFM: effects of relative humidity, particle size and wall adhesion. Powder Technol. 132, 196–210.
20) Kainer, K.U., 2006. Metal Matrix Composites: Custom-made Materials for Automotive and Aerospace Engineering. John Wiley & Sons.
21) Karnezis, P.A., Durrant, G., Cantor, B., 1998. Characterization of reinforcement distribution in cast Al-Alloy/ SiCp composites. Mater. Charact. 40, 97–109.
22) Lin, C.B., Hung, Y.W., Liu, W., Kang, S., 2001. Machining and fluidity of 356Al/SiC(p) composites. J. Mater. Process. Technol. 110, 152–159.
23) Lin, H., Hwu, W., Ger, M., 2008. The dispersion of silver nanoparticles with physical dispersal procedures. J. Mater. Process. Technol. 206, 56–61.
24) Lloyd, D., 1994. Particle reinforced aluminium and magnesium matrix composites. Int. Mater. Rev. 39, 1–23.
25) Lloyd, D., 1991. Aspects of fracture in particulate reinforced metal matrix composites. Acta Metall. Mater. 39, 59–71.
26) Lloyd, D., 1989. The solidification microstructure of particulate reinforced aluminium/ SiC composites. Composites Sci Technol 35, 159–179.
27) Madhu, H.C., Ajay Kumar, P., Perugu, C.S., Kailas, S.V., 2018. Microstructure and mechanical properties of friction stir process derived Al-TiO2 nanocomposite. J. Mater. Eng. Perform. 27, 1318–1326.
28) Matsumoto, A., Kobayashi, K., Nishio, T., Ozaki, K., 2003. Fabrication and thermal expansion of Al-ZrW2O8 composites by pulse current sintering process. Mater Sci Forum 426-432, 2279–2284.
29) Miranda, A.T., Bolzoni, L., Barekar, N., Huang, Y., Shin, J., Ko, S., et al., 2018. Processing, structure and thermal conductivity correlation in carbon fibre reinforced aluminium metal matrix composites. Mater. Des. 156, 329–339.
30) Mooney, M., 1951. The viscosity of a concentrated suspension of spherical particles. J. Colloid Sci. 6, 162–170.
31) Nieto, A., Yang, H., Jiang, L., Schoenung, J.M., 2017. Reinforcement size effects on the abrasive wear of boron carbide reinforced aluminum composites. Wear 390–391, 228–235.
32) AK, P., Raj, R., Kailas, S.V., 2015. A novel in-situ polymer derived nano ceramic MMC by friction stir processing. Mater. Des. 85, 626–634.
33) Patel, J., Zuo, Y., Fan, Z., Krane, M., Jardy, A., Williamson, R., et al., 2013. Liquid Metal Engineering by Application of Intensive Melt Shearing. pp. 291–299.
34) Ravi, K., Pillai, R., Amaranathan, K., Pai, B., Chakraborty, M., 2008. Fluidity of aluminum alloys and composites: a review. J Alloys Compounds 456, 201–210.
35) Ravi, K., Pillai, R., Pai, B., Chakraborty, M., 2007. Influence of Interfacial Reaction on the Fluidity of A356 Al-SiCp Composites—A Theoretical Approach. Metall. Mater. Trans. A 38, 2531–2539.
36) Rogers, A., 1974. Statistical Analysis of Spatial Dispersion: the Quadrat Method. Pion.
37) Rohatgi, P., 1980. Fluidity of mica particle dispersed aluminium alloy. J. Mater. Sci. 15, 2777–2784.
38) Rumpf, H., 1962. The strength of granules and agglomerates. In: Knepper, W.A. (Ed.), Agglomeration. Wiley, New York, U. S. A, pp. 379–418.
39) Sannino, A.P., Rack, H.J., 1995. Dry sliding wear of discontinuously reinforced aluminum composites: review and discussion. Wear 189, 1–19.
40) Sreekumar, V., Babu, N.H., Eskin, D., Fan, Z., 2015. Structure–property analysis of in-situ Al–MgAl 2 O 4 metal matrix composites synthesized using ultrasonic cavitation. Mater. Sci. Eng. A 628, 30–40.
41) Sritharan, T., Chan, L., Tan, L., Hung, N., 2001. A feature of the reaction between Al and SiC particles in an MMC. Mater. Charact. 47, 75–77.
42) Srivatsan, T.S., Al-Hajri, M., Smith, C., Petraroli, M., 2003. The tensile response and fracture behavior of 2009 aluminum alloy metal matrix composite. Mater. Sci. Eng. A 346, 91–100.
43) Taylor, J., 1996. Metal-related castability effects in aluminium foundry alloys. Cast Met. 8, 225–252.
44) Thakur, S.K., Dhindaw, B.K., 2001. The influence of interfacial characteristics between SiC p and Mg/Al

metal matrix on wear, coefficient of friction and microhardness. Wear 247, 191–201.
45) Timelli, G., Bonollo, F., 2007. Fluidity of aluminium die castings alloy. Int. J. Cast Met. Res. 20, 304–311.
46) Tjong, S., Lau, K., 2000. Abrasion resistance of stainless-steel composites reinforced with hard TiB 2 particles. Composites Sci Technol 60, 1141–1146.
47) Utomo, A., Baker, M., Pacek, A., 2009. The effect of stator geometry on the flow pattern and energy dissipation rate in a rotor–stator mixer. Chem. Eng. Res. Des. 87, 533–542.
48) Wang, J., Guo, Q., Nishio, M., Ogawa, H., Shu, D., Li, K., et al., 2003. The apparent viscosity of fine particle reinforced composite melt. J. Mater. Process. Technol. 136, 60–63.
49) Wolfenden, A., Oliver, K., Singh, M., 1996. Measurements of elastic and anelastic properties of reaction-formed silicon carbide ceramics. J. Mater. Sci. 31, 6073–6076.
50) Yalcin, Y., Akbulut, H., 2006. Dry wear properties of A356-SiC particle reinforced MMCs produced by two melting routes. Mater. Des. 27, 872–881.
51) Yang, X., Huang, Y., Barekar, N.S., Das, S., Stone, I.C., Fan, Z., 2016. High shear dispersion technology prior to twin roll casting for high performance magnesium/ SiCp metal matrix composite strip fabrication. Compos. Part A Appl. Sci. Manuf. 90, 349–358.
52) Yarandi, F., Rohatgi, P., Ray, S., 1993. Fluidity and microstructure formation during flow of Al-SiC particle composites. J. Mater. Eng. Perform. 2, 359–364.
53) Yarnadi, F., 1991. Melting and casting characteristics of Al A-356 SiC particulate reinforced cast composites. Melt and Casting Characterisitics of Al A356 SiC Particulate Reinforced Cast Composites. University of Wisconsin-Milwaukee PhD thesis.
54) Zhang, J., Perez, R.J., Lavernia, E.J., 1994. Effect of SiC and graphite particulates on the damping behavior of metal matrix composites. Acta Metall. Mater. 42, 395–409.